HHS Public Access

Author manuscript

ACS Chem Biol. Author manuscript; available in PMC 2020 April 19.

Published in final edited form as:

ACS Chem Biol. 2019 April 19; 14(4): 665–673. doi:10.1021/acschembio.8b01044.

Hyperpolarized [6-^{13}C,$^{15}N_3$]-Arginine as a Probe for *in Vivo* Arginase Activity

Andrew Cho[†,‡], **Roozbeh Eskandari**[§], **Kristin L. Granlund**[§], and **Kayvan R. Keshari**[*,†,§,‖]

[†]Department of Biochemistry and Structural Biology, Weill Cornell Graduate School, New York, New York 10065, United States

[‡]Weill Cornell/Rockefeller/Sloan Kettering Tri-Institutional MD-PhD Program, New York, New York 10065, United States

[§]Department of Radiology, Memorial Sloan Kettering Cancer Center, New York, New York 10065, United States

[‖]Molecular Pharmacology Program, Memorial Sloan Kettering Cancer Center, New York, New York 10065, United States

Abstract

Alterations in arginase enzyme expression are linked with various diseases and have been shown to support disease progression, thus motivating the development of an imaging probe for this enzymatic target. ^{13}C-enriched arginine can be used as a hyperpolarized (HP) magnetic resonance (MR) probe for arginase flux since the arginine carbon-6 resonance (157 ppm) is converted to urea (163 ppm) following arginase catalyzed hydrolysis. However, scalar relaxation from adjacent ^{14}N-nuclei shortens cabon-6 T_1 and T_2 times, yielding poor spectral properties. To address these limitations, we report the synthesis of [6-^{13}C,$^{15}N_3$]-arginine and demonstrate that ^{15}N-enrichment increases carbon-6 relaxation times, thereby improving signal-to-noise ratio and spectral resolution. By overcoming these limitations with this novel isotope-labeling scheme, we were able to perform *in vitro* and *in vivo* arginase activity measurements with HP MR. We present HP [6-^{13}C,$^{15}N_3$]-arginine as a noninvasive arginase imaging agent for preclinical studies, with the potential for future clinical diagnostic use.

[*]**Corresponding Author**: rahimikk@mskcc.org.

Supporting Information

The Supporting Information is available free of charge on the ACS Publications website at DOI: 10.1021/acschembio.8b01044. Detailed methods for the *in vivo* [6-^{13}C,$^{15}N_3$]-arginine tracing experiment and complete synthetic methods for each intermediate, including yields, ^{1}H and ^{13}C NMR data, and high-resolution mass spectrometry data (PDF)

The authors declare the following competing financial interest(s): K.R.K. serves on the scientific advisory board for NVision Imaging Technologies.

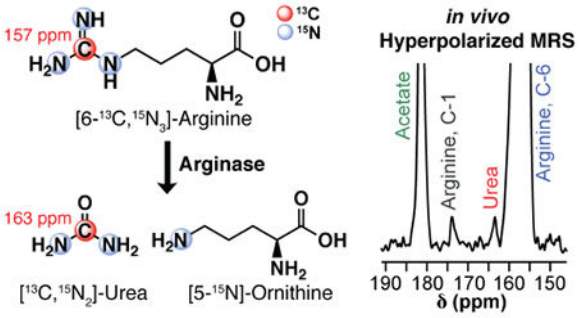

Arginine is a proteinogenic amino acid with a wide range of metabolic fates. One such fate is its hydrolysis to urea and ornithine, which is enzymatically catalyzed by one of two arginase isoforms (Figure 1).[1,2] Arginase-1 is involved in the urea cycle and is therefore heavily expressed in liver cells, whereas arginase-2 is present to a lesser degree across a variety of tissue types.[2] This enzymatic activity is of particular interest because aberrations in arginase expression are associated with a variety of pathologies, including liver disease,[3] psoriasis,[4] pulmonary diseases,[5] inflammatory bowel disease,[6] and cancer.[7] Specifically with respect to cancer, urea cycle metabolism as a whole can be rewired to facilitate the metabolic needs of the proliferating cell. Arginase presents an entry into the urea cycle via the production of ornithine, which subsequently participates in a cascade of metabolic processes whose role in cancer progression is still under investigation. Researchers have recently increased efforts toward this end and found correlations between alterations in arginase expression and disease progression across an array of cancer subtypes.[8–11] For instance, arginase-2 expression in breast cancer has been shown to promote cell proliferation, with arginase inhibition yielding dampened growth rates.[12,13] Clinical studies on breast cancer patients have also demonstrated that serum arginase activity correlates with elevated histological grade.[14,15] Aside from arginase expression in cancer cells themselves, elevated arginase-1 expression in tumor associated macrophages is thought to support an immunosuppressive phenotype that promotes T-cell evasion and tumor growth.[16,17] Thus, there is a strong link between disease progression and arginase expression, and the development of an imaging agent for arginase activity will address an unmet need of significant relevance to biomedical research.

Hyperpolarized (HP) ^{13}C magnetic resonance imaging (MRI) is an appropriate imaging modality for this application, as it can be used to quantify enzymatic flux in regions of interest throughout the body.[18] With this technique, the nuclear spin polarization of a ^{13}C-enriched molecule can be transiently enhanced to increase its ^{13}C-MR signal.[19] The HP state facilitates rapid acquisition of high signal-to-noise ratio (SNR) spectra, which can be used to monitor enzymatic conversion of the HP molecule to downstream metabolites in real time. This method has been used to measure enzyme kinetics *in vitro*, as well as to measure flux through enzymatic pathways *in vivo*.[20–22] However, the exponential decay constant of the HP state is typically on the order of 10s of seconds for ^{13}C-nuclei,[23] so only rapid enzymatic processes can be studied with this technique.

To date, a molecular imaging probe to directly assess *in vivo* arginase activity has not been developed. A prior study with [6-^{13}C]-arginine demonstrated that the carbon-6 resonance of this compound can be hyperpolarized and used to detect arginase-catalyzed hydrolysis of arginine to urea.[24] However, the presence of three directly bonded ^{14}N quadrupole nuclei (I = 1, 99.6% natural abundance) introduces scalar relaxation to the carbon-6 resonance.[25] This causes shortened T_1 in very low magnetic fields (e.g., during transfer of a HP sample from the polarizer to the MRI), resulting in increased sample depolarization prior to data acquisition. Furthermore, scalar relaxation shortens T_2 relaxation times at both low and high magnetic field strengths, resulting in broadening of resonance peak widths. Collectively, the effect of scalar relaxation on the $T1$ and T_2 of the carbon-6 resonance of [6-^{13}C]-arginine contributes to lower SNR, making *in vivo* translation of this molecule challenging.

These limitations motivated the design and synthesis of [6-^{13}C,^{15}N$_3$]-arginine (Figure 2), in which the three guanidino nitrogen are enriched with ^{15}N to dramatically decrease scalar relaxation on the carbon-6 resonance. This yields enhanced spectral properties and lowers the barrier for *in vivo* translation, and we report a convergent synthetic scheme for [6-^{13}C, ^{15}N$_3$]-arginine in this Article. Following synthesis of this compound, T_1 and T_2 values of the carbon-6 resonance of [6-^{13}C,^{15}N$_3$]- and [6-^{13}C]-arginine were measured to assess the effect of ^{15}N-enrichment on ^{13}C relaxation times. In addition, enzyme kinetic parameters for recombinant arginase-1 were measured using natural abundance arginine or [6-^{13}C,^{15}N$_3$]-arginine as the substrate to evaluate the kinetic isotope effect of heavy-atom enrichment. Conversion of HP [6-^{13}C,^{15}N$_3$]-arginine to [^{13}C,^{15}N$_2$]-urea was detected *in vitro* as well as *in vivo* in a proof-of-concept magnetic resonance spectroscopy (MRS) study. Our results demonstrate that the spectral properties of the carbon-6 resonance of arginine can be improved by reducing ^{14}N-mediated scalar relaxation, ultimately facilitating *in vivo* detection of arginase flux.

RESULTS AND DISCUSSION

Heavy-Atom Labeling of Arginine Does Not Significantly Alter Arginase Enzyme Kinetics.

On the basis of previously solved crystal structures of human arginase-1 complexed with several different arginase inhibitors, a mechanism for arginase-catalyzed hydrolysis of arginine has been proposed in which His, Glu, Asp, and 2 Mn^{2+} ions at the arginase active site coordinate with the guanidino group of arginine.[26] Heavy-isotope enrichment can decrease enzymatic rates as a function of the kinetic isotope effect,[27] and we suspected that arginase-1 kinetics will be impaired when acting on [6-^{13}C,^{15}N$_3$]-arginine since the sites of heavy-atom enrichment are at or near the sites of coordination with the arginase-1 active site.

Enzyme kinetics for recombinant human arginase-1 using either [6-^{13}C,^{15}N$_3$]-arginine or natural abundance (unenriched) arginine were fit to the Michaelis–Menten kinetics model and are reported in Figure 3A. These results show that K_m values do not significantly differ between the two analogs (95% confidence intervals are 2.17 ± 0.51 mM for unenriched arginine, and 2.04 ± 0.55 mM for [6-^{13}C,^{15}N$_3$]-arginine), whereas there is a 12% decrease in V_{max} when the enzyme acts on heavy-atom enriched arginine (95% confidence intervals are 54.8 ± 4.26 s^{-1} for unenriched arginine and 48.2 ± 4.17 s^{-1} for [6-^{13}C,^{15}N$_3$]-arginine).

While this decrease in V_{max} ($p = 0.029$, extra sum-of-squares F-test, d.f. = 22) is consistent with the proposed arginase mechanism of action and should be noted, it is not large enough to be prohibitive toward HP enzymatic flux studies.

^{15}N-Enrichment Mitigates Scalar Relaxation, and the Carbon-6 Resonance of [6-^{13}C,$^{15}N_3$]-Arginine Can Be Hyperpolarized by dDNP.

Thermal equilibrium T_1 and T_2 relaxation times of the arginine carbon-6 resonance were measured at 14.1 T_1 revealing that ^{15}N-enrichment at the guanidino group does not extend T_1 (95% confidence intervals are 7.21 ± 0.14 s with enrichment and 7.18 ± 0.18 s without) but yields a significant increase in T_2 (95% confidence intervals are 0.488 ± 0.012 s with enrichment and 0.174 ± 0.004 s without, $p < 0.0001$, extra sum-of-squares F-test, d.f. = 18) (Figure 3B,C), and these values are consistent with previously reported values.[28] These trends are also in accordance with the phenomenon that scalar relaxation effects on T_1 are highly field dependent and pronounced at very low fields, in contrast to its effects on T_2.[25]

A similar trend regarding T_2* was also observed at 1 T when comparing line widths from a thermal equilibrium ^{13}C NMR spectrum containing a mixture of [6-^{13}C]- and [6-^{13}C,$^{15}N_3$]-arginine (Figure 3D). Note that the carbon-6 resonance of [6-^{13}C,$^{15}N_3$]-arginine is a quartet due to coupling with ^{15}N. Since the full-width-half-max (fwhm) of a resonant peak is inversely proportional to T_2*, we compared the fwhm of the carbon-6 resonance of both species to measure relative differences in T_2* at 1 T. As B_0-inhomogeneity can decrease T_2*, both compounds were mixed together in a single NMR tube so sample-to-sample differences in B_0-inhomogeneity could be ignored when interpreting differences in peak widths. The fwhm values of each of the split carbon-6 resonances of [6-^{13}C,$^{15}N_3$]-arginine, from downfield to upfield, were 1.34, 1.68, 1.76, and 1.38 Hz, whereas the fwhm for [6-^{13}C]-arginine was measured to be 3.16 Hz. The fwhm values of the ^{15}N-enriched variant were roughly half that of the unenriched variant, indicating that ^{15}N-enrichment increases T_2*, and probably also T_2, of the carbon-6 resonance at 1 T.

HP T_1 of the carbon-6 resonance of arginine was also measured at 1 T, starting roughly at 20–30 s post-dissolution. The dynamic HP ^{13}C NMR acquisition in Figure 3E shows T_1 relaxation of the hyperpolarized carbon-6 resonance of [6-^{13}C,$^{15}N_3$]-arginine at 157 ppm (T_1 = 15.13 ± 1.23 s, $n = 4$), and the T_1 is consistent with a previously published measurement.[28] Meanwhile, the carbon-6 resonance of [6-^{13}C]-arginine could not be detected due to rapid scalar-mediated relaxation at low field during sample transfer. Carbon-6 polarization of [6-^{13}C,$^{15}N_3$]-arginine at the time of dissolution was calculated to be 6.51% ± 0.85%, $n = 4$, but this value could not be calculated for [6-^{13}C]-arginine.

For both molecules, HP signal from natural abundance ^{13}C at the carbon-1 position was also observed at 175 ppm, suggesting both [6-^{13}C]- and [6-^{13}C,$^{15}N_3$]-arginine were polarized to similar levels but the carbon-6 resonance of [6-^{13}C]-arginine rapidly depolarized during sample transfer. We previously reported that the carbon-6 HP T_1 relaxation times of both arginine species are similar at 1 T,[28] so the loss of carbon-6 polarization is likely due to strong scalar-mediated relaxation from ^{14}N on carbon-6 polarization at very low magnetic fields.

The improved relaxation properties of [6-^{13}C,$^{15}N_3$]-arginine make it potentially superior to [6-^{13}C]-arginine for spectroscopic imaging applications. The drastic reduction in scalar relaxation via ^{15}N-enrichment results in increased T_2 relaxation times, facilitating implementation of longer spectral readout times and longer echo-trains to yield improved spectral resolution and increased imaging resolution, respectively. Though the carbon-6 T_1 values of both variants are similar at 1 T, the absence of rapid scalar-mediated depolarization at low field in [6-^{13}C,$^{15}N_3$]-arginine makes this molecule better equipped for *in vivo* translation. The dramatic reduction in low field scalar relaxation makes it easier to transfer the sample from the polarizer to the MRI without substantial hyperpolarization loss. Although a rapid-injection system can be used to circumvent this issue for preclinical studies, it is likely difficult to translate [6-^{13}C]-arginine for clinical studies, regardless of the method used for hyperpolarization, since rapid injection cannot be used. On the basis of current practices, HP clinical samples must undergo a quality control process during which samples are analyzed at low field for upward of 1 min prior to injection into a patient.[29,30] During this time, [6-^{13}C]-arginine would rapidly depolarize via ^{14}N-mediated scalar relaxation, whereas this depolarization mechanism is minimized in ^{15}N-enriched arginine.

Conversion of HP [6-^{13}C,$^{15}N_3$]-Arginine to [^{13}C,$^{15}N_2$]-Urea Scales with Increasing Arginase Activity in Liver Homogenates.

Since the liver endogenously expresses high amounts of arginase-1 due to its role in the urea cycle, mouse liver homogenate was used to demonstrate that arginase-mediated conversion of HP [6-^{13}C,$^{15}N_3$]-arginine to [^{13}C,$^{15}N_2$]-urea could be detected with ^{13}C NMR and that this conversion scales with enzymatic activity. Furthermore, since the arginase-1 activate site contains two paramagnetic Mn^{2+} ions, which coordinate with the arginine side chain, we also sought to determine whether the presence of these paramagnetic metals depolarizes ^{13}C-hyperpolarization when HP [6-^{13}C,$^{15}N_3$]-arginine is bound to the arginase active site. HP [6-^{13}C,$^{15}N_3$]-arginine was mixed with varying amounts of mouse liver homogenate, and ^{13}C-spectra were acquired every 3 s (Figure 4A). The seven spectra from Figure 4A were summed and are shown in Figure 4B, and the ratio of the urea AUC to the arginine carbon-1 AUC is reported in Figure 4C.

It is important to note that increasing the amount of liver homogenate also increases the levels of free metals and proteins in the sample, whose presence shortens ^{13}C-T_1, and we hypothesize this accounts for the total ^{13}C-signal decrease in the sample with more liver homogenate. To address this, we normalized the urea signal to the carbon-1 signal, as opposed to the carbon-6 signal of arginine, since the former exhibits a longer T_1 and will undergo a smaller relative change in T_1 as levels of liver homogenate are increased. The results from Figure 4 demonstrate that arginase-catalyzed hydrolysis of HP [6-^{13}C,$^{15}N_3$]-arginine can be detected with NMR, production of [^{13}C,$^{15}N_2$]-urea scales with arginase activity ($p = 0.0078$, two-tailed t test, d.f. = 2, Figure 4C), and the presence of Mn^{2+} in the arginase active site does not completely depolarize arginine hyperpolarization during catalysis.

In Vivo Arginase Activity Can Be Detected with HP [6-^{13}C,$^{15}N_3$]-Arginine.

For a proof-of-concept demonstration of *in vivo* arginase activity detection with HP [6-^{13}C, $^{15}N_3$]-arginine, a healthy female athymic nude mouse was used. From our earlier imaging attempts with HP [6-^{13}C,$^{15}N_3$]-arginine, we noticed that anesthesia with isoflurane significantly increased the toxicity of intravenously administered arginine in mice. We observed that a 250 μL bolus of 10–30 mM arginine could be lethal to an anesthetized mouse under isoflurane but was nontoxic when the same dose was intravenously administered to an awake mouse. To limit the use of anesthesia and reduce arginine toxicity during HP MRI scans, we adapted a previously reported method of awake animal restraint for ophthalmologic imaging applications, in which mice were restrained in a plastic Mouse DecapiCone Restrainer (Braintree Scientific).[31]

A slab dynamic acquisition across a 2 cm axial slice containing the entire liver and superior region of the kidneys (Figure 5A) was performed to detect *in vivo* conversion of HP [6-^{13}C, $^{15}N_3$]-arginine to [^{13}C,$^{15}N_2$]-urea. ^{13}C-spectra were acquired every 2 s and are shown in Figure 5B, displaying the arrival, accumulation, and signal decay of HP [6-^{13}C,$^{15}N_3$]-arginine in the excitation slice. When the spectra are magnified and summed, the HP signal from [^{13}C,$^{15}N_2$]-urea and carbon-1 of arginine (natural abundance ^{13}C) can also be seen (Figure 5C,D). To further verify these findings, we infused mice with [6-^{13}C,$^{15}N_3$]-arginine, collected liver and serum samples 90 s post-infusion, and acquired ^{13}C NMR on *ex vivo* liver and serum metabolite extracts. [^{13}C,$^{15}N_2$]-urea was detected in both tissues, with liver and serum urea concentrations corresponding to 1.51% ± 0.59% and 1.26% ± 0.14% of the total injected arginine dose per gram of tissue, respectively, and no [6-^{13}C,$^{15}N_3$]-arginine was detected in the liver (Figure S1). These results suggest that metabolism through arginase is highly active in the murine liver since [^{13}C,$^{15}N_2$]-urea could be detected in the serum and liver within 90 s post-injection, similar to what was observed with *in vivo* HP MRI. In addition, the inability to detect [6-^{13}C,$^{15}N_3$]-arginine in *ex vivo* liver extract implies that arginine is rapidly converted to urea upon uptake into the liver, suggesting that the [6-^{13}C, $^{15}N_3$]-arginine signal in the *in vivo* data set is predominantly from [6-^{13}C,$^{15}N_3$]-arginine in the blood. This proof-of-concept experiment demonstrates that *in vivo* conversion of arginine to urea in the mouse liver can be detected with HP [6-^{13}C,$^{15}N_3$]-arginine, paving the way for future arginase imaging experiments on different tissues/pathologies and with increased imaging resolution.

Conclusions.

We report a high-yield, multistep synthesis for [6-^{13}C,$^{15}N_3$]-arginine from commercially available precursors. Though [6-^{13}C]-arginine is commercially available, scalar relaxation from three covalently bound ^{14}N-nuclei on carbon-6 results in shortened T_1 and T_2. Our results demonstrate that ^{15}N-enrichment of the three directly bonded nitrogen improves SNR and spectral resolution as a function of decreased scalar relaxation, and future studies will be aimed at utilizing the increased ^{13}C-T_2 to achieve increased imaging resolution. This work highlights the advantages of ^{15}N-enrichment for HP probes with ^{13}C-enrichment on amidelike functionalities, and similar benefits should be appreciated when applying this technique to other HP probes with this functional group, such as glutamine,[32] thiourea,[33] small peptides,[34,35] and amino acid derivatives.[36–38] Heavy-atom enrichment at 4 positions

in [6-^{13}C,$^{15}N_3$]-arginine results in impaired arginase enzyme kinetics, but the decrease in V_{max} is on the order of ~10% and does not prohibit HP enzyme kinetics studies. Furthermore, the conversion rate of HP [6-^{13}C,$^{15}N_3$]-arginine to HP [^{13}C,$^{15}N_2$]-urea scales with arginase activity *in vitro*, and this enzymatic process can also be detected in healthy mouse liver *in vivo*. This work represents the first demonstration of noninvasive, *in vivo* detection of arginase activity, in part facilitated by the improved spectral properties afforded from ^{15}N-enrichment. As researchers continue to study the role of urea cycle rewiring, or specifically arginase activity, in disease progression, HP [6-^{13}C,$^{15}N_3$]-arginine can be used as an additional tool to advance this research. In addition, since our imaging approach is clinically translatable, it is possible that HP [6-^{13}C,$^{15}N_3$]-arginine can be used to image arginase flux in humans in the future.

Future endeavors with this probe will involve deeper ventures into biological applications and imaging, consisting of more comprehensive studies in biological systems as well as further improvements to spectral properties and data acquisition. With respect to biology, we aim to explore the use of this probe in the setting of disease, such as cancer, to determine whether it can be used as a clinically relevant prognostic marker. In addition, we intend to take advantage of the long carbon-6 T_2 and explore the use of longer echo-train acquisitions with increased imaging resolution. The use of a ^{15}N-decoupler will further unlock the potential of this probe, as it will collapse the carbon-6 quartet to a singlet, increasing SNR by a factor of ~2 and improving spectral resolution. Implementation of ^{1}H-decoupling to improve the *in vivo* SNR of HP ^{13}C-MRS experiments has been previously reported,[39] and we believe a similar setup can be used to facilitate ^{15}N-decoupling. Arginine variants with different heavy-atom labeling schemes, as well as other amino acids, can also be synthesized by implementing minor changes to the scheme in Figure 2A due to the modular nature of our synthetic route. For example, deuteration at the carbon-5 position can be easily achieved by replacing H_2 with D_2 in step h. This may yield even longer carbon-6 relaxation times because splitting between carbon-5 protons and carbon-6 is observed as a triplet in ^{13}C NMR when ^{1}H-decoupling is turned off (Supporting Information), suggesting that carbon-5 protons may be close enough to exhibit significant dipolar relaxation on cabon-6.

Applications of [6-^{13}C,$^{15}N_3$]-arginine are also not just limited to HP ^{13}C NMR or MRI. Since ^{15}N itself is MR-active, this molecule may be used to assay arginase flux via detection of HP ^{15}N resonances. Though the receptivity of ^{15}N is lower than ^{13}C, this may be compensated by the propensity of ^{15}N-nuclei to exhibit longer T_1. This probe can also be used in the non-HP setting, as [6-^{13}C,$^{15}N_3$]-arginine can be injected intravenously or added to tissue culture media, after which ^{13}C NMR of tissue extracts, cell extracts, or cell media can be performed to follow the metabolic fates of arginine. Due to the ^{13}C- and ^{15}N-labeling scheme of [6-^{13}C,$^{15}N_3$]-arginine, the arginine carbon-6 resonance and resulting urea carbon resonance exhibit characteristic splitting with ^{15}N, allowing unambiguous detection of [^{13}C, $^{15}N_2$]-urea produced from [6-^{13}C,$^{15}N_3$]-arginine with ^{13}C NMR, as demonstrated in Figure S1. In theory, this logic can be employed to follow arginine metabolism to creatine, agmatine, and citrulline, but this has yet to be demonstrated. Aside from MR applications, this molecule can also be used for mass spectrometry-based metabolic tracing studies via detection of ^{13}C- and ^{15}N-enrichment in downstream metabolites. This can be applied to metabolic tracing of [6-^{13}C,$^{15}N_3$]-arginine in *in vitro* cell culture or *ex vivo* tissue extracts,[40]

as well as to newer techniques such as *ex vivo* metabolite imaging of tissue slices or cells with desorption electrospray ionization (DESI)[41] imaging or multi-isotope imaging mass spectrometry (MIMS)[42] for more spatially resolved analysis of metabolism. Overall, this work highlights the potential of [6-^{13}C,$^{15}N_3$]-arginine as an *in vivo* HP imaging probe, and future experiments will be designed toward further exploring the utility of this molecule.

METHODS

Synthesis of [6-^{13}C,$^{15}N_3$]-Arginine HCl.

The synthetic scheme for [6-^{13}C,$^{15}N_3$]-arginine is detailed in Figure 2 and was adapted from previously published work on similar compounds.[43,44] Each reaction in the multistep synthesis was optimized to >50% yield, with a total overall yield of 9.42%. The final product was purified via crystallization as the monohydrochloride salt. Reaction conditions, ^{1}H and ^{13}C NMR spectra, and high-resolution mass spectrometry results for each intermediate are listed in the Supporting Information.

T_2 and T_2 Measurements at 14.1 T.

A 14.1 T NMR spectrometer (Bruker) was used to measure thermal equilibrium T_1 and T_2 relaxation times of the carbon-6 resonance of [6-^{13}C,$^{15}N_3$]-arginine and [6-^{13}C]-arginine. Each compound was dissolved to a final concentration of 20 mM in a 1:9 (v/v) solution consisting of D_2O and 100 mM Tris, 1 mM EDTA, pH 7.4, in H_2O. D_2O was added to the mixture to facilitate spin-locking to minimize B_0 drift. For T_1 calculation, ^{13}C NMR spectra were acquired using a standard inversion recovery sequence with a 52631.578 Hz spectral width, 65 536 points, and delay times ranging from 2 to 30 s between the 180° and 90° pulses. Spectra for T_2 calculation were acquired using a Carr–Purcell–Meiboom–Gill (CPMG) sequence on the same samples. Each CPMG spectrum was acquired with a 50 000 Hz spectral width, 16 384 points, and 0.01 s echo time. Total echo times between 0.02 and 0.8 s were sampled. Each inversion recovery and CPMG acquisition was an average of 12 scans, and a >5 × T_1 wait time was implemented between scans to allow full recovery of longitudinal magnetization. For the T_1 calculation, the area under the curve (AUC) of the carbon-6 resonance from each inversion recovery spectrum was integrated in MNova[45] (Mestrelabs) and AUC values were plotted against delay time in Prism 7[46] (GraphPad Software) for curve fitting. For the T_2 calculation, the AUC of the carbon-6 resonance from each CPMG spectrum was integrated and AUC values were plotted against total echo time for curve fitting. AUC vs time was fit to a monoexponential function to calculate T_1 and T_2, and values are reported with a 95% confidence interval.

Hyperpolarization of [6-^{13}C,$^{15}N_3$]-Arginine.

For all HP experiments, [6-^{13}C,$^{15}N_3$]-arginine HCl or [6-^{13}C]-arginine HCl (Cambridge Isotope Laboratories) was dissolved to a final concentration of 3.2 M in deionized H_2O in the presence of 1 equiv of HCl and 15–20 mM OX063 radical (General Electric). The sample was sonicated at 45 °C for 1 h and subsequently polarized with dissolution dynamic nuclear polarization (dDNP) in a General Electric 5T SPINlab Polarizer (>2 h, 0.8 K, 139.960 GHz) for *in vivo* experiments or a General Electric 3.35T SPINlab Polarizer (>1 h, 0.8 K, 93.980 GHz) for all other experiments. Following polarization, the HP substrate was

expelled from the polarizer via rapid dissolution, during which the HP sample is dissolved in a superheated aqueous solution of 100 mM Tris, 1 mM EDTA, pH 7.4, and ejected into a prechilled vial (−20 °C) containing 1 equiv of 10 N NaOH. For *in vivo* experiments, the dissolution buffer was prepared in D_2O.

Polarization Level, HP T_1, and Line Width Measurements at 1 T.

All 1 T measurements were acquired on a Magritek SpinSolve 1 T ^{13}C NMR spectrometer. All spectra were acquired with a 2500 Hz spectral width and 4096 points. For HP T_1 measurements of the carbon-6 resonances of [6-^{13}C]-arginine and [6-^{13}C,$^{15}N_3$]-arginine, each substrate was polarized separately and dissolved to a final concentration of 10–15 mM upon dissolution. For each measurement, 300 μL of the HP dissolution was added to a 5 mm NMR tube and was loaded in the spectrometer approximately 20–30 s post-dissolution. Spectra were acquired every 3 s with a 10° or 30° excitation. T_1 values were calculated by plotting the AUC values of the resonance of interest against time and fitting the points to a monoexponential decay function in Prism 7,[46] which was corrected for polarization loss from each excitation.[28,47]

^{13}C polarization levels were approximated by comparing the carbon-6 AUC from the first HP spectrum with the thermal equilibrium carbon-6 AUC of the same sample. For thermal equilibrium measurements, the HP sample was allowed to depolarize to thermal equilibrium polarization, after which a solution of 0.5 M Gd-DOTA in H_2O was added to a final concentration of 1 mM. A ^{13}C NMR spectrum was subsequently acquired using a Magritek SpinSolve 1 T spectrometer with a 90° excitation and 10 s repetition time and averaged over 8192 scans. Polarization levels were calculated by multiplying the ^{13}C polarization levels at 1 T and 300 K (calculated as 0.000086% on the basis of the Boltzmann distribution) with the fold-enhancement of the HP signal versus the thermal equilibrium signal, and this value was subsequently extrapolated back to the initial time of dissolution using the measured T_1 at 1 T. The final polarization value was corrected for differences in excitation angle and number of averages between the two measurements.

To compare differences in T_2* between [6-^{13}C,$^{15}N_3$]-arginine and [6-^{13}C]-arginine, a solution containing 40 mM of each compound was prepared in 1:9 D_2O/100 mM Tris, 1 mM EDTA (pH 7.4) in H_2O. A ^{13}C NMR spectrum of this mixture was averaged over 119 298 scans with a 45° excitation and 5 s repetition time. Fwhm measurements of the carbon-6 resonances were measured in MNova[45] and used to compare T_2* between the two species.

Colorimetric Arginase Activity Assay.

A previously described 96-well plate-based colorimetric assay for quantitative urea detection[48,49] was used to measure enzyme kinetics of recombinant human arginase-1 enzyme (Abcam). Each well contained 10 ng of arginase-1, 40 mM Tris (pH 7.4), 0.4 mM EDTA, and natural abundance or [6-^{13}C,$^{15}N_3$]-arginine ranging from 0.25 to 10 mM in a final volume of 60 μL. Each condition was loaded in a 96-well plate in triplicate and incubated at 37 °C for 40 min before quenching the enzymatic reaction with sulfuric acid and assaying for urea via 530 nm wavelength absorbance, as previously described.[48,49] Since arginine also absorbs at 530 nm, blanks for each concentration of arginine were

prepared in triplicate. Absorbance values were referenced to a urea standard curve ranging from 0 to 500 μM urea, and these values were used for K_m and V_{max} calculations.

Arginase Activity Measurement in Murine Liver Homogenate with HP [6-^{13}C,$^{15}N_3$]-Arginine.

Liver tissue was collected from male SCID mice and stored in a −80 °C freezer prior to homogenization. For homogenate preparation, 260 mg of liver was mixed with 520 μL of RIPA lysis and extraction buffer containing 0.5 mM EDTA and supplemented with protease and phosphatase inhibitors (Thermo Fisher Scientific). This mixture was incubated on ice for 5 min, blended with a hand-held tissue homogenizer, and incubated on ice for another 30 min. The solution was subsequently pelleted in a microcentrifuge at 14000 rpm and 4 °C for 30 min, and the supernatant was collected for HP enzymatic activity assays.

For HP arginase activity measurements, Eppendorf tubes were filled with either 10 or 30 μL of liver homogenate (corresponding to 3.3 or 10 μg of liver, respectively), and an aqueous solution of 100 mM Tris (pH 7.4), 1 mM EDTA was added to each tube to bring the total volume up to 100 μL. This mixture was equilibrated to 37 °C in a water bath prior to dissolution of the HP substrate. Following polarization, HP [6-^{13}C,$^{15}N_3$]-arginine was dissolved to a final concentration ranging from 11.13 to 16.56 mM after dissolution. 200 μL of the [6-^{13}C,$^{15}N_3$]-arginine dissolution was mixed with the liver homogenate solution and transferred to a clean NMR tube. A total of seven 1 T ^{13}C NMR spectra were acquired starting 15 s post-mixing using a 30° excitation every 3 s. Each spectrum was acquired with a 2500 Hz spectral width and 4096 points. Free induction decays (FIDs) were zero-filled to 65 536 points and line broadened with a 1.5 Hz filter during post-processing, prior to analysis and quantification. Each condition was measured in triplicate.

In Vivo Arginase Flux Measurement (3 T MRI).

The imaging experiment was conducted with a Bruker 3T preclinical MRI equipped with a dual-tuned ^{1}H/^{13}C coil. The lateral tail vein of a female athymic nude mouse (7 months old, Charles River) was cannulated with a 28 cm 23-gauge rodent tail vein catheter (Braintree Scientific). The catheter was pre-filled with 10 U heparin mL^{-1} in normal saline, which was used to prevent coagulation within the catheter, and the mouse was anesthetized using a continuous flow of 1 L min^{-1} oxygen with 1.5% isoflurane. Once unconscious, the mouse was placed in a DecapiCone restrainer (Braintree Scientific) and loaded on the MRI bed, which was equipped with a water heater and nose cone for continued delivery of 1.5% isoflurane. A 4 M [1-^{13}C]-acetate phantom was placed adjacent the mouse for ^{13}C pulse calibration. The mouse was subsequently loaded inside the MRI, and its abdomen was centered within the coil. The magnetic field was shimmed throughout a 2 cm slice containing the mouse liver and kidneys. Five minutes before dissolution, isoflurane was removed to allow the mouse to regain consciousness while restrained in the DecapiCone in the MRI. HP [6-^{13}C,$^{15}N_3$]-arginine was dissolved to a final concentration of 26 mM after dissolution, and the mouse was injected with 250 μL of this solution through the catheter over 10 s. Note that this injected volume excludes the 100 μL of 10 U heparin mL^{-1} in the dead volume of the catheter, which was also injected into the mouse. A slab dynamic acquisition was initiated just prior to injection, similar to previously reported methods.[32,50,51] During acquisition, a ^{13}C spectrum was acquired across the shimmed 2 cm slice

every 2 s with a 30° excitation, 4132 Hz spectral width, and 4096 points. Isoflurane was readministered after the HP scan; the unconscious mouse was taken out of the MRI and restrainer, and the cannula was removed while the animal was sedated. *In vivo* MRS data was post-processed with previously reported noise thresholding,[52] after which FIDs were truncated to 512 points to match the T_2^* decay and eliminate noise from the end of the acquisition window, zero-filled to 4096 points, and line broadened with a 20 Hz filter.

Supplementary Material

Refer to Web version on PubMed Central for supplementary material.

ACKNOWLEDGMENTS

We would like to thank G. Sukenick and the Memorial Sloan Kettering Nuclear Magnetic Resonance Core for helpful advice with NMR experiments and high-resolution mass spectrometry measurements. This work was supported by the National Institutes of Health, F30 CA225174 (AC.), T32 GM007739 (A.C. and K.R.K.), and P30 CA008748 (K.R.K.), the Tow Foundation Postdoctoral Fellowship (R.E.), the Ludwig Center for Basic and Translational Immunology (K.R.K.), Geoffrey Beene Cancer Research Center (K.R.K.), and the Thompson Family Foundation (K.R.K.).

REFERENCES

(1). Morris SM (2007) Arginine Metabolism: Boundaries of Our Knowledge. J. Nutr 137, 1602S–1609S. [PubMed: 17513435]

(2). Flynn NE, Meininger CJ, Haynes TE, and Wu G (2002) The Metabolic Basis of Arginine Nutrition and Pharmacotherapy. Biomed. Pharmacother 56, 427–438. [PubMed: 12481979]

(3). Maier KP, Talke H, and Gerok W (1979) Activities of Urea-Cycle Enzymes in Chronic Liver Disease. Klin. Wochenschr 57, 661–665. [PubMed: 225605]

(4). Bruch-gerharz D, Schnorr O, Suschek C, Beck K, Pfeilschifter J, Ruzicka T, and Kolb-bachofen V (2003) Arginase 1 Overexpression in Psoriasis. Am. J. Pathol 162, 203–211. [PubMed: 12507903]

(5). Maarsingh H, Pera T, and Meurs H (2008) Arginase and Pulmonary Diseases. Naunyn-Schmiedeberg's Arch. Pharmacol 378, 171–184. [PubMed: 18437360]

(6). Horowitz S, Binion DG, Nelson VM, Kanaa Y, Javadi P, Lazarova Z, Andrekopoulos C, Kalyanaraman B, Otterson MF, and Rafiee P (2007) Increased Arginase Activity and Endothelial Dysfunction in Human Inflammatory Bowel Disease. AJP-Gastrointest Liver Physiol 292, G1323–G1336.

(7). Keshet R, Szlosarek P, Carracedo A, and Erez A (2018) Rewiring Urea Cycle Metabolism in Cancer to Support Anabolism. Nat. Rev. Cancer 18, 634–645. [PubMed: 30194362]

(8). Chaerkady R, Harsha HC, Nalli A, Gucek M, Vivekanandan P, Akhtar J, Cole RN, Simmers J, Schulick RD, Singh S, Torbenson M, Pandey A, and Thuluvath PJ (2008) A Quantitative Proteomic Approach for Identification of Potential Biomarkers in Hepatocellular Carcinoma. J. Proteome Res 7, 4289–4298. [PubMed: 18715028]

(9). Zaytouni T, Tsai P, Hitchcock DS, Dubois CD, Freinkman E, Lin L, Morales-Oyarvide V, Lenehan PJ, Wolpin BM, Mino-Kenudson M, Torres EM, Stylopoulos N, Clish CB, and Kalaany NY (2017) Critical Role for Arginase 2 in Obesity-Associated Pancreatic Cancer. Nat. Commun 8, 242. [PubMed: 28808255]

(10). Ochocki JD, Khare S, Hess M, Ackerman D, Qiu B, Daisak JI, Worth AJ, Lin N, Lee P, Xie H, Li B, Wubbenhorst B, Maguire TG, Nathanson KL, Alwine JC, Blair IA, Nissim I, Keith B, and Simon MC (2018) Arginase 2 Suppresses Renal Carcinoma Progression via Biosynthetic Cofactor Pyridoxal Phosphate Depletion and Increased Polyamine Toxicity. Cell Metab. 27, 1263–1280. [PubMed: 29754953]

(11). Poillet-Perez L, Xie X, Zhan L, Yang Y, Sharp DW, Hu ZS, Su X, Maganti A, Jiang C, Lu W, Zheng H, Bosenberg MW, Mehnert JM, Guo JY, Lattime E, Rabinowitz JD, and White E (2018) Autophagy Mantains Tumor Growth Through Circulating Arginine. Nature 563, 569. [PubMed: 30429607]

(12). Singh R, Pervin S, Wu G, and Chaudhuri G (2001) Activation of Caspase-3 Activity and Apoptosis in MDA-MB-468 Cells by N^{ω}-Hydroxy-L-Arginine, an Inhibitor of Arginase, Is Not Solely Dependent on Reduction in Intracellular Polyamines. Carcinogenesis 22, 1863–1869. [PubMed: 11698350]

(13). Singh R, Avliyakulov NK, Braga M, Haykinson MJ, Martinez L, Singh V, Parveen M, Chaudhuri G, and Pervin S (2013) Proteomic Identification of Mitochondrial Targets of Arginase in Human Breast Cancer. PLoS One 8, e79242. [PubMed: 24223914]

(14). Porembska Z, Luboiński G, Chrzanowska A, Mielczarek M, Magnuska J, and Baranńczyk-Kuźma A (2003) Arginase in Patients with Breast Cancer. Clin. Chim. Acta 328, 105–111. [PubMed: 12559605]

(15). Perez G, Olivares IM, Rodriguez MG, Ceballos GM, and Sanchez JRG (2012) Arginase Activity in Patients with Breast Cancer: An Analysis of Plasma, Tumors, and Its Relationship with the Presence of the Estrogen Receptor. Onkologie 35, 570–574. [PubMed: 23038227]

(16). Rodriguez PC, Quiceno DG, Zabaleta J, Ortiz B, Zea AH, Piazuelo MB, Delgado A, Correa P, Brayer J, Sotomayor EM, Antonia S, Ochoa JB, and Ochoa AC (2004) Arginase I Production in the Tumor Microenvironment by Mature Myeloid Cells Inhibits T-Cell Receptor Expression and Antigen-Specific T-Cell Responses. Cancer Res. 64, 5839–5849. [PubMed: 15313928]

(17). Colegio OR, Chu N-Q, Szabo AL, Chu T, Rhebergen AM, Jairam V, Cyrus N, Brokowski CE, Eisenbarth SC, Phillips GM, Cline GW, Phillips AJ, and Medzhitov R (2014) Functional Polarization of Tumour-Associated Macrophages by Tumour-Derived Lactic Acid. Nature 513, 559–563. [PubMed: 25043024]

(18). Comment A, and Merritt ME (2014) Hyperpolarized Magnetic Resonance as a Sensitive Detector of Metabolic Function. Biochemistry 53, 7333–7357. [PubMed: 25369537]

(19). Ardenkjær-Larsen JH, Fridlund B, Gram A, Hansson G, Hansson L, Lerche MH, Servin R, Thaning M, and Golman K (2003) Increase in Signal-to-Noise Ratio of > 10,000 Times in Liquid-State NMR. Proc. Natl. Acad. Sci. U. S. A 100, 10158–10163. [PubMed: 12930897]

(20). Cho A, Lau JYC, Geraghty BJ, Cunningham CH, and Keshari KR (2017) Noninvasive Interrogation of Cancer Metabolism with Hyperpolarized 13C MRI. J. Nucl. Med 58, 1201–1206. [PubMed: 28596156]

(21). Kurhanewicz J, Vigneron DB, Brindle K, Chekmenev EY, Comment A, Cunningham CH, Deberardinis RJ, Green GG, Leach MO, Rajan SS, Rizi RR, Ross BD, Warren WS, and Malloy CR (2011) Analysis of Cancer Metabolism by Imaging Hyperpolarized Nuclei: Prospects for Translation to Clinical Research. Neoplasia 13, 81–97. [PubMed: 21403835]

(22). Schroeder MA, Clarke K, Neubauer S, and Tyler DJ (2011) Hyperpolarized Magnetic Resonance: A Novel Technique for the *In Vivo* Assessment of Cardiovascular Disease. Circulation 124, 1580–1594. [PubMed: 21969318]

(23). Keshari KR, and Wilson DM (2014) Chemistry and Biochemistry of ^{13}C Hyperpolarized Magnetic Resonance Using Dynamic Nuclear Polarization. Chem. Soc. Rev 43, 1627–1659. [PubMed: 24363044]

(24). Najac C, Chaumeil MM, Kohanbash G, Guglielmetti C, Gordon JW, Okada H, and Ronen SM (2016) Detection of Inflammatory Cell Function Using ^{13}C Magnetic Resonance Spectroscopy of Hyperpolarized [6-^{13}C]-Arginine. Sci. Rep 6, 31397. [PubMed: 27507680]

(25). Chiavazza E, Kubala E, Gringeri CV, Düwel S, Durst M, Schulte RF, and Menzel MI (2013) Earth's Magnetic Field Enabled Scalar Coupling Relaxation of ^{13}C Nuclei Bound to Fast-Relaxing Quadrupolar ^{14}N in Amide Groups. J. Magn. Reson 227, 35–38. [PubMed: 23262330]

(26). Di Costanzo L, Sabio G, Mora A, Rodriguez PC, Ochoa AC, Centeno F, and Christianson DW (2005) Crystal Structure of Human Arginase I at 1.29-Å Resolution and Exploration of Inhibition in the Immune Response. Proc. Natl. Acad. Sci. U. S. A 102, 13058–13063. [PubMed: 16141327]

(27). Schmitt JA, Myerson AL, and Daniels F (1952) Relative Rates of Hydrolysis of Urea Containing C^{14}, C^{13} and C^{12}. J. Phys. Chem 56, 917–920.

(28). Cho A, Eskandari R, Miloushev VZ, and Keshari KR (2018) A Non-Synthetic Approach to Extending the Lifetime of Hyperpolarized Molecules Using D_2O Solvation. J. Magn. Reson 295, 57–62. [PubMed: 30099234]

(29). Nelson SJ, Kurhanewicz J, Vigneron DB, Larson PEZ, Harzstark AL, Ferrone M, van Criekinge M, Chang JW, Bok R, Park I, Reed G, Carvajal L, Small EJ, Munster P, Weinberg VK, Ardenkjaer-Larsen JH, Chen AP, Hurd RE, Odegardstuen L-I, Robb FJ, Tropp J, and Murray JA (2013) Metabolic Imaging of Patients with Prostate Cancer Using Hyperpolarized [1-^{13}C]Pyruvate. Sci. Transl. Med 5, 198ra108.

(30). Miloushev VZ, Granlund KL, Boltyanskiy R, Lyashchenko SK, DeAngelis LM, Mellinghoff IK, Brennan CW, Tabar V, Yang TJ, Holodny AI, Sosa RE, Guo YW, Chen AP, Tropp J, Robb F, and Keshari KR (2018) Metabolic Imaging of the Human Brain with Hyperpolarized ^{13}C Pyruvate Demonstrates ^{13}C Lactate Production in Brain Tumor Patients. Cancer Res. 78, 3755–3760. [PubMed: 29769199]

(31). Cohan BE, et al. (2003) Optic Disc Imaging in Conscious Rats and Mice. Invest. Ophthalmol. Visual Sci. 44, 160–163.

(32). Cabella C, Karlsson M, Canapè C, Catanzaro G, Serra SC, Miragoli L, Poggi L, Uggeri F, Venturi L, Jensen PR, Lerche MH, and Tedoldi F (2013) *In Vivo* and *in Vitro* Liver Cancer Metabolism Observed with Hyperpolarized [5-^{13}C]Glutamine. J. Magn. Reson 232, 45–52. [PubMed: 23689113]

(33). Wibowo A, Park JM, Liu S-C, Khosla C, and Spielman DM (2017) Real-Time *in Vivo* Detection of H2O2 Using Hyperpolarized ^{13}C-Thiourea. ACS Chem. Biol 12, 1737–1742. [PubMed: 28452454]

(34). Jamin Y, Gabellieri C, Smyth L, Reynolds S, Robinson SP, Springer CJ, Leach MO, Payne GS, and Eykyn TR (2009) Hyperpolarized ^{13}C Magnetic Resonance Detection of Carboxypeptidase G2 Activity. Magn. Reson. Med 62, 1300–1304. [PubMed: 19780183]

(35). Hata R, Nonaka H, Takakusagi Y, Ichikawa K, and Sando S (2016) Design of a Hyperpolarized Molecular Probe for Detection of Aminopeptidase N Activity. Angew. Chem., Int. Ed 55, 1765–1768.

(36). Wilson DM, Hurd RE, Keshari K, Van Criekinge M, Chen AP, Nelson SJ, Vigneron DB, and Kurhanewicz J (2009) Generation of Hyperpolarized Substrates by Secondary Labeling with [1,1-^{13}C] Acetic Anhydride. Proc. Natl. Acad. Sci. U. S. A 106, 5503–5507. [PubMed: 19276112]

(37). Flavell RR, Von Morze C, Blecha JE, Korenchan DE, Van Criekinge M, Sriram R, Gordon JW, Chen H, Subramaniam S, Bok RA, Wang ZJ, Vigneron DB, Larson PE, Kurhanewicz J, and Wilson DM (2015) Application of Good's Buffers to pH Imaging Using Hyperpolarized ^{13}C MRI. Chem. Commun 51, 14119–14122.

(38). Hundshammer C, Düwel S, Ruseckas D, Topping G, Dzien P, Müller C, Feuerecker B, Hövener JB, Haase A, Schwaiger M, Glaser SJ, and Schilling F (2018) Hyperpolarized Amino Acid Derivatives as Multivalent Magnetic Resonance PH Sensor Molecules. Sensors 18, 600.

(39). Chen AP, Tropp J, Hurd RE, Van Criekinge M, Carvajal LG, Xu D, Kurhanewicz J, and Vigneron DB (2009) *In Vivo* Hyperpolarized ^{13}C MR Spectroscopic Imaging with ^{1}H Decoupling. J. Magn. Reson 197, 100–106. [PubMed: 19112035]

(40). Buescher JM, Antoniewicz MR, Boros LG, Burgess SC, Brunengraber H, Clish CB, DeBerardinis RJ, Feron O, Frezza C, Ghesquiere B, Gottlieb E, Hiller K, Jones RG, Kamphorst JJ, Kibbey RG, Kimmelman AC, Locasale JW, Lunt SY, Maddocks ODK, Malloy C, Metallo CM, Meuillet EJ, Munger J, Nöh K, Rabinowitz JD, Ralser M, Sauer U, Stephanopoulos G, St-Pierre J, Tennant DA, Wittman C, Vander Heiden MG, Vazquez A, Vousden K, Young JD, Zamboni N, and Fendt S-M (2015) A Roadmap for Interpreting ^{13}C Metabolite Labeling Patterns from Cells. Curr. Opin. Biotechnol 34, 189–201. [PubMed: 25731751]

(41). Wiseman JM, Ifa DR, Zhu Y, Kissinger CB, Manicke NE, Kissinger PT, and Cooks RG (2008) Desorption Electrospray Ionization Mass Spectrometry: Imaging Drugs and Metabolites in Tissues. Proc. Natl. Acad. Sci. U. S. A 105, 18120–18125. [PubMed: 18697929]

(42). Steinhauser ML, Bailey AP, Senyo SE, Guillermier C, Perlstein TS, Gould AP, Lee RT, and Lechene CP (2012) Multi-Isotope Imaging Mass Spectrometry Quantifies Stem Cell Division and Metabolism. Nature 481, 516–519. [PubMed: 22246326]

(43). Qu W, Zha Z, Lieberman BP, Mancuso A, Stetz M, Rizzi R, Ploessl K, Wise D, Thompson C, and Kung HF (2011) Facile Synthesis [5-^{13}C-4-$^{2}H_2$]-L-Glutamine for Hyperpolarizd MRS Imaging of Cancer Metabolism. Acad. Radiol 18, 932–939. [PubMed: 21658976]

(44). Hamilton DJ, and Sutherland A (2004) A Flexible Approach for the Synthesis of Selectively Labelled L-Arginine. Tetrahedron Lett. 45, 5739–5741.

(45). Cobas C, Domínguez S, Larin N, Iglesias I, Geada C, Seoane F, Sordo M, Monje P, Fraga S, Cobas R, Peng C, Fraga D, García JA, Goebel M, Vaz E, Ovchinnikov O, Barba A, and Sant OL MestReNova, Mestrelab Research S.L, 2015.

(46). Radushev D Prism 7 for Mac OS X, GraphPad Software, Inc, 2016.

(47). Tee SS, DiGialleonardo V, Eskandari R, Jeong S, Granlund KL, Miloushev V, Poot AJ, Truong S, Alvarez JA, Aldeborgh HN, and Keshari KR (2016) Sampling Hyperpolarized Molecules Utilizing a 1 T Permanent Magnetic Field. Sci. Rep 6, 32846. [PubMed: 27597137]

(48). Knipp M, and Vasák M (2000) A Colorimetric 96-Well Microtiter Plate Assay for the Determination of Enzymatically Formed Citrulline. Anal. Biochem 286, 257–264. [PubMed: 11067748]

(49). Stone EM, Glazer VS, Chantranupong L, Cherukuri P, Breece RM, Tierney DL, Curley SA, Iverson BL, and Georgiou G (2010) Replacing Mn^{2+} with Co^{2+} in Human Arginase I Enhances Cytotoxicity toward L-Arginine Auxotrophic Cancer Cell Lines. ACS Chem. Biol 5, 333–342. [PubMed: 20050660]

(50). Albers MJ, Bok R, Chen AP, Cunningham CH, Zierhut ML, Zhang VY, Kohler SJ, Tropp J, Hurd RE, Yen YF, Nelson SJ, Vigneron DB, and Kurhanewicz J (2008) Hyperpolarized ^{13}C Lactate, Pyruvate, and Alanine: Noninvasive Biomarkers for Prostate Cancer Detection and Grading. Cancer Res. 68, 8607–8615. [PubMed: 18922937]

(51). Chaumeil MM, Larson PEZ, Yoshihara HAI, Danforth OM, Vigneron DB, Nelson SJ, Pieper RO, Phillips JJ, and Ronen SM (2013) Non-Invasive *in Vivo* Assessment of IDH1Mutational Status in Glioma. Nat. Commun 4, 2429. [PubMed: 24019001]

(52). Doyle M, Chapman BLW, Balschi JA, and Pohost GM (1994) SIFT, a Postprocessing Method That Increases the Signal-to-Noise Ratio of Spectra Which Vary in Time. J. Magn. Reson., Ser. B 103, 128–133.

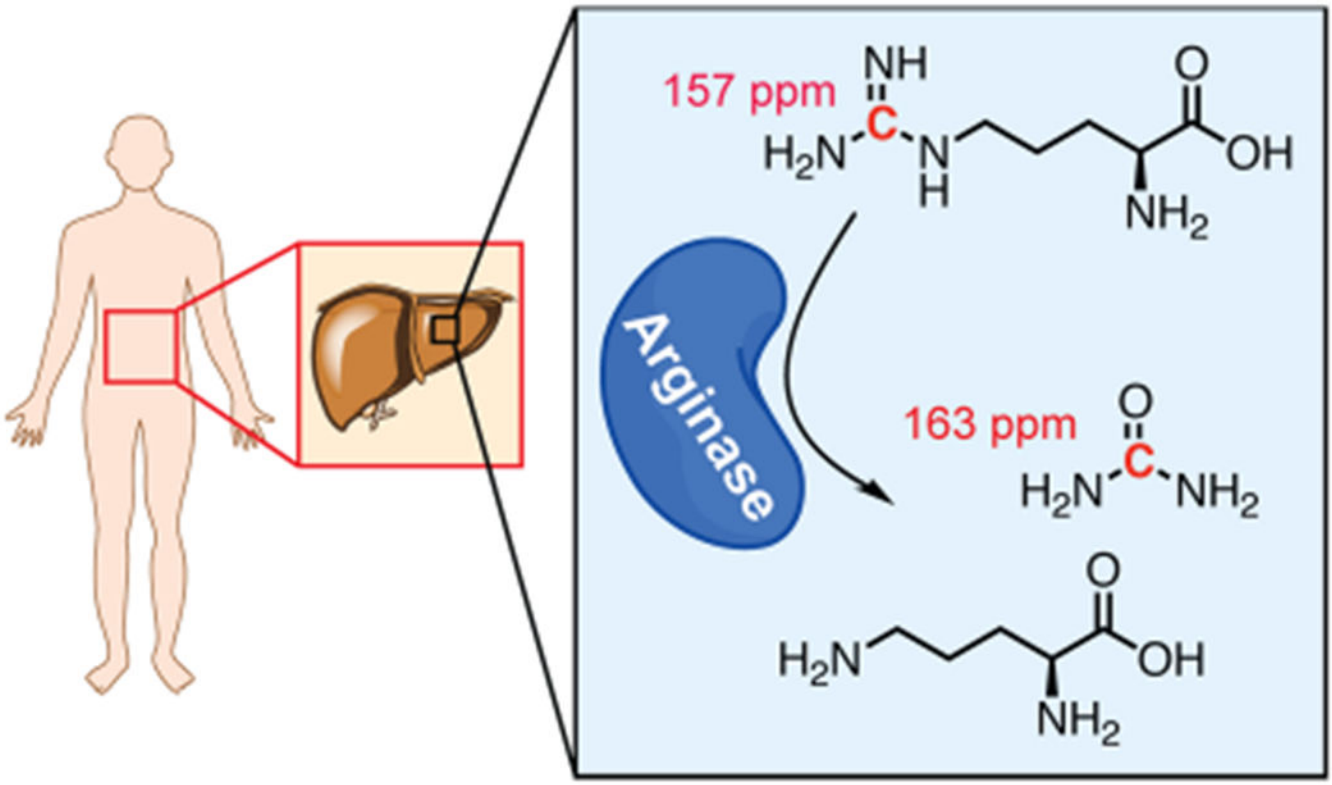

Figure 1.

General scheme of arginase-catalyzed hydrolysis of arginine. Liver arginase hydrolyzes arginine (top) to urea (middle) and ornithine (bottom). Chemical shift values of the specified carbon resonances are indicated in red.

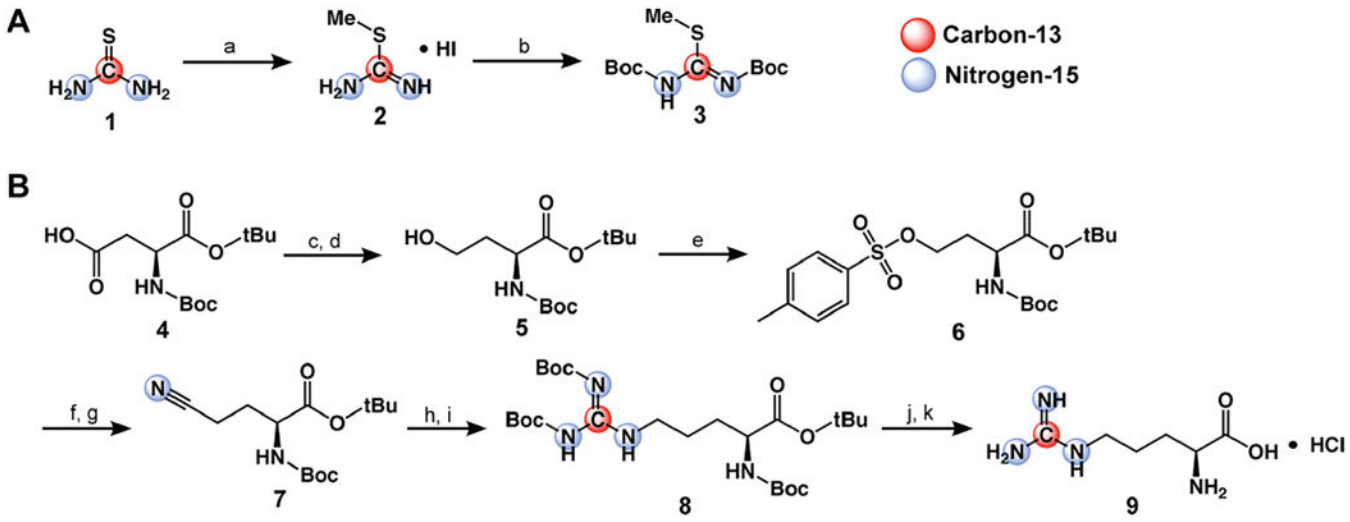

Figure 2.

Synthesis of [6-^{13}C,^{15}N$_3$]-arginine. (A) Synthetic scheme for Boc-protected thiourea-derived precursor (compound **3**). (a) 1.15 equiv of CH_3I, EtOH, reflux, 3 h; (b) 4 equiv of Boc_2O, DCM, sat. $NaHCO_3$, RT, 5 d. (B) Synthetic scheme for [6-^{13}C,^{15}N$_3$]-arginine. (c) 1.5 equiv of ECF, 1.5 equiv of Et_3N, THF, −10 °C → RT, 30 min; (d) 2.1 equiv of $NaBH_4$, THF/H_2O, 0 °C → RT, 1 h; (e) 2 equiv of TsCl, 5 equiv of Et_3N, 0.1 equiv of DMAP, DCM, 0 °C → RT, 1 h; (f) 2 equiv of NaI, acetone, reflux, 1 h; (g) 1.2 equiv of KC^{15}N, DMSO, 80 °C, 18 h; (h) H_2, Pd/C, AcOH, RT, 2 h; (i) 1 equiv of compound **3**, 5 equiv of Et_3N, DMSO, RT, 24 h; (j) 1:9 TFA/DCM, RT, 18 h; (k) 1 M HCl.

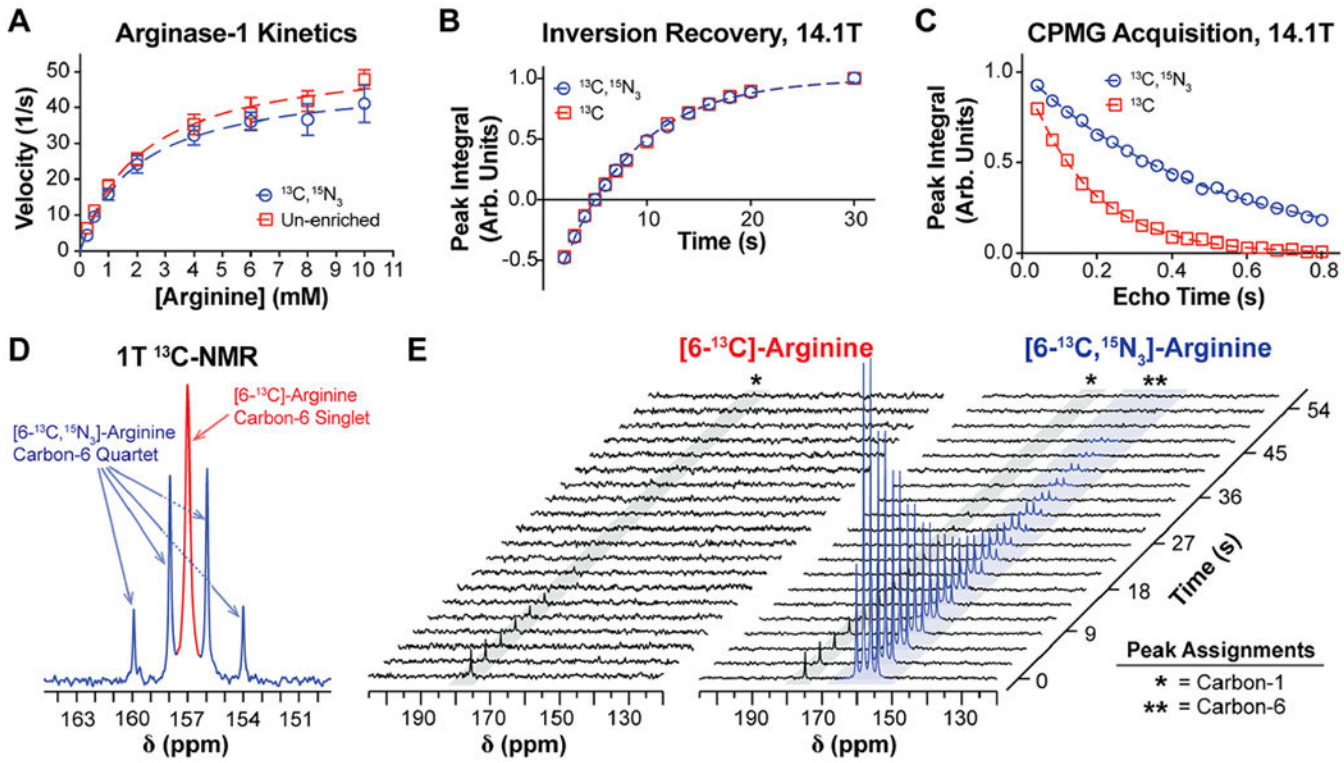

Figure 3.

Biochemical and spectroscopic properties of [6-^{13}C,^{15}N$_3$]-arginine. (A) Enzyme kinetics of recombinant human arginase-1, using either natural abundance arginine (red) or [6-^{13}C,^{15}N$_3$]-arginine (blue) as the enzymatic substrate. Data points were fit to the Michaelis–Menten kinetics model (dashed lines) to approximate K_m and V_{max}, revealing no significant difference in K_m but a significant 13% decrease in V_{max} with isotopic enrichment. (B) Inversion recovery and (C) CPMG acquisitions on the carbon-6 resonance of each arginine variant at 14.1 T, which were used to measure T_1 and T_2, respectively. At 14.1 T, ^{15}N-enrichment does not increase carbon-6 T_1 but it yields a roughly 3-fold increase in T_2. (D) 1 T ^{13}C NMR spectrum of an aqueous equimolar mixture of [6-^{13}C]- and [6-^{13}C,^{15}N$_3$]-arginine, displaying the carbon-6 resonance of each arginine variant. Peak widths were quantified to approximate relative differences in carbon-6 T_2*, and the narrower peak widths for [6-^{13}C,^{15}N$_3$]-arginine indicate an increase in T_2* with ^{15}N-enrichment. (E) 1 T ^{13}C NMR of HP [6-^{13}C]- and [6-^{13}C,^{15}N$_3$]-arginine acquired with a 30° excitation every 3 s. Scalar-mediated relaxation from adjacent ^{14}N-nuclei results in depolarization of the carbon-6 resonance of [6-^{13}C]-arginine during sample transfer from the polarizer to the spectrometer, whereas this relaxation mechanism is mitigated in [6-^{13}C,^{15}N$_3$]-arginine.

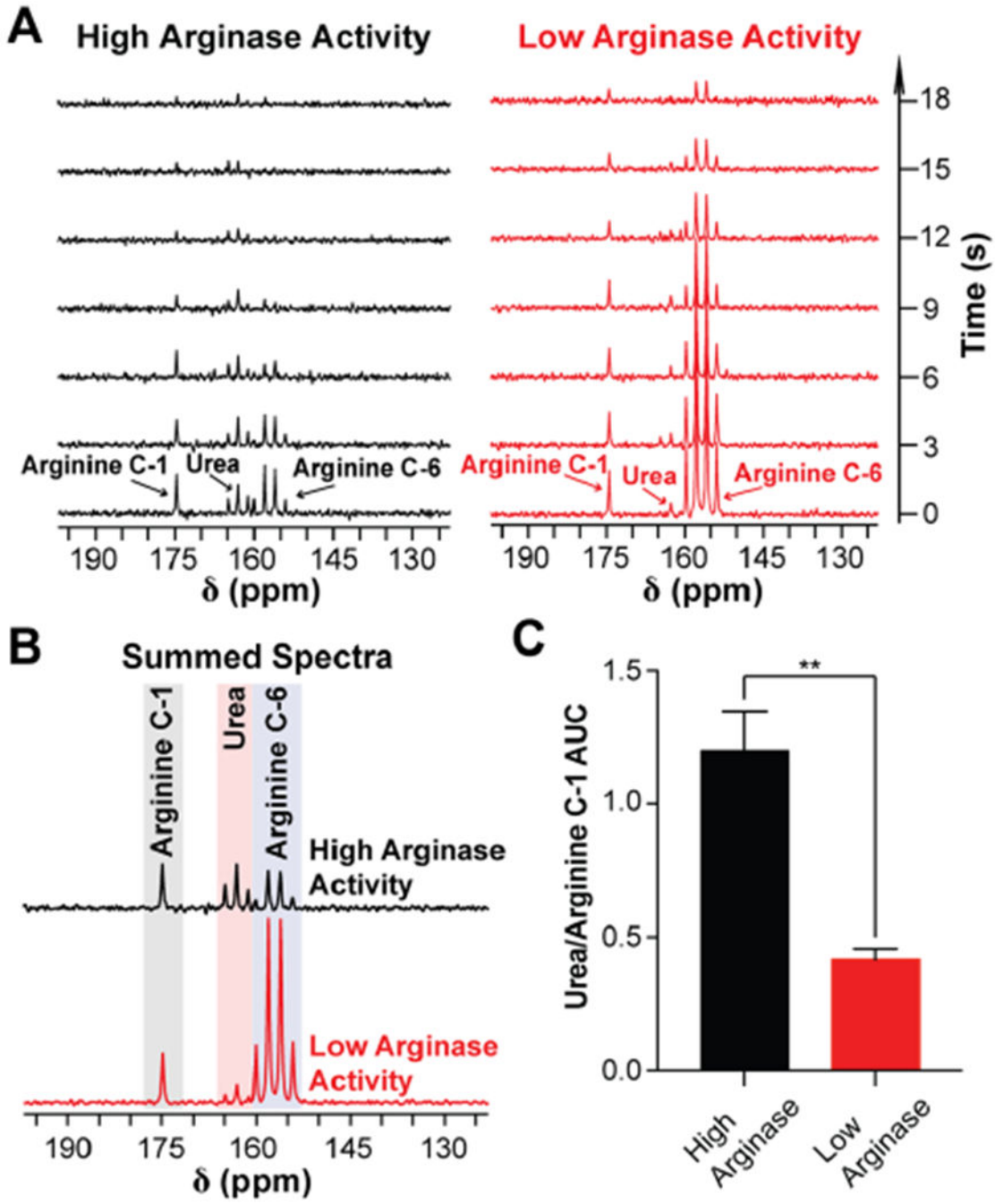

Figure 4.

Arginase-catalyzed hydrolysis of HP [6-^{13}C,$^{15}N_3$]-arginine to [^{13}C,$^{15}N_2$]-urea can be detected with 1 T NMR. (A) 1 T ^{13}C NMR of HP [6-^{13}C,$^{15}N_3$]-arginine mixed with either high levels (left, homogenate containing 10 μg of mouse liver) or low levels (right, homogenate containing 3.3 μg of mouse liver) of arginase activity, demonstrating that HP [^{13}C,$^{15}N_2$]-urea production scales with increasing arginase activity. Spectra were acquired with a 30° excitation every 3 s. (B) Sum of the spectra from (A). (C) Ratio of the urea peak integral with the carbon-1 resonance of arginine from (B). $^{**}p < 0.01$.

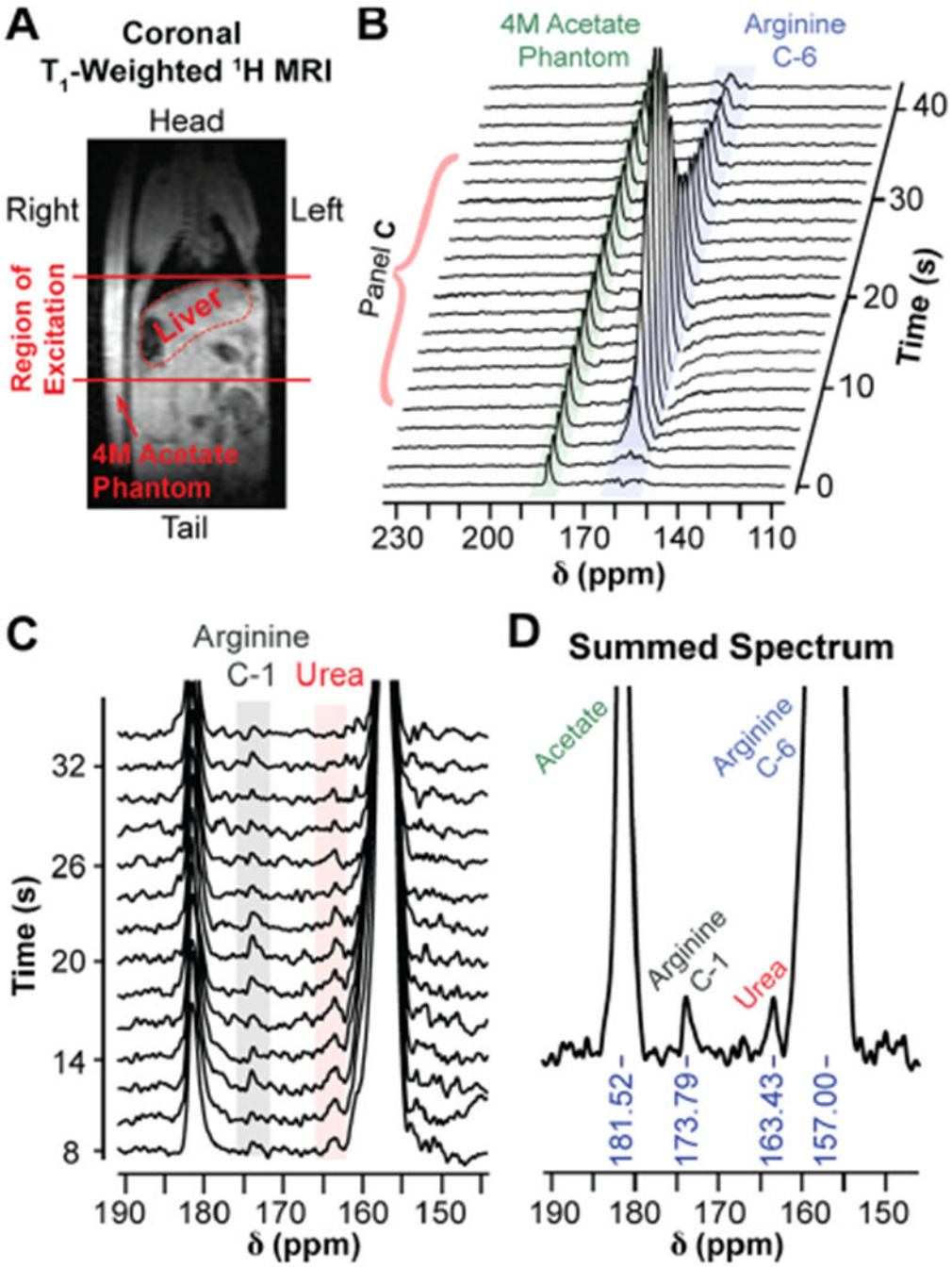

Figure 5.

In vivo detection of liver arginase activity with HP [6-^{13}C,^{15}N$_3$]-arginine. (A) Coronal T_1-weighted ^{1}H-MRI of a female athymic nude mouse placed next to a 4 M [1-^{13}C]-acetate phantom. The 2 cm region of excitation for HP ^{13}C-MRS acquisition is indicated by the solid red lines. (B) ^{13}C-spectra from the 2 cm region indicated in (A) following injection with HP [6-^{13}C,^{15}N$_3$]-arginine, acquired with a 30° excitation every 2 s. The spectra illustrate the accumulation and subsequent signal decay of [6-^{13}C,^{15}N$_3$]-arginine within the excitation slice. (C) Spectra 5–18 from (B), magnified to display the arginine carbon-1

(natural abundance) and urea resonances. The urea resonance is likely from arginase-mediated hydrolysis of hyperpolarized [6-^{13}C,$^{15}N_3$]-arginine in the liver. Spectra have been baseline corrected with cubic splines. (D) Sum of spectra 5–18 from (B). The resulting summed spectrum was baseline corrected with cubic splines.